

# Model for Dynamic Self-Assembled Magnetic Surface Structures

M. Belkin,<sup>1,2</sup> A. Glatz,<sup>2</sup> A. Snezhko,<sup>2</sup> and I.S. Aranson<sup>2</sup>

<sup>1</sup>*Department of Chemical Engineering, Northwestern University, 2145 Sheridan Rd, Evanston, IL 60208*

<sup>2</sup>*Materials Science Division, Argonne National Laboratory, 9700 South Cass Avenue, Argonne, IL 60439*

(Dated: November 20, 2018)

We propose a first-principles model for self-assembled magnetic surface structures on the water-air interface reported in earlier experiments [1, 2]. The model is based on the Navier-Stokes equation for liquids in shallow water approximation coupled to Newton equations for interacting magnetic particles suspended on the water-air interface. The model reproduces most of the observed phenomenology, including spontaneous formation of magnetic snake-like structures, generation of large-scale vortex flows, complex ferromagnetic-antiferromagnetic ordering of the snake, and self-propulsion of bead-snake hybrids. The model provides valuable insights into self-organization phenomena in a broad range of non-equilibrium magnetic and electrostatic systems with competing interactions.

PACS numbers: 87.19.ru; 43.35.Lf; 75.50.Tt; 47.63.Gd

Understanding the fundamental principles governing dynamic self-assembly in non-equilibrium systems continues attracting enormous attention in physics and engineering communities [1–8]. The interest is stimulated by the need for creating smart, dynamic materials capable of self-assembly, adaptation to environments, and for the design of artificial structures capable of performing useful tasks on the microscale [9, 10], including targeted cargo delivery [11] or stirring in microfluidic devices [12].

In a series of works [1, 2] we reported experimental studies of self-assembled dynamic magnetic microstructures (magnetic snakes) formed on the water-air interface from a dispersion of magnetic particles energized by an alternating (*ac*) magnetic field applied perpendicular to the interface. The snakes form due to coupling between the fluid's surface deformations and the collective response of particles to an *ac* magnetic field. These spectacular dynamic structures have complex magnetic ordering [13]: the snakes' segments are formed by ferromagnetically aligned chains of microparticles; however, the segments are always anti-ferromagnetically ordered, see Fig. 1. The snakes generate two pairs of large-scale vortices located at the tails. Under certain conditions snakes spontaneously break the symmetry of the vortex pairs and turn into self-propelled entities [2, 14]. Some aspect of the snakes' behavior were reproduced by phenomenological models based on the Ginzburg-Landau type equation for surface waves coupled to a large-scale flow [2]. Nevertheless, the fundamental microscopic mechanisms leading to the formation of snakes and the relation between properties of the snakes and microscopic properties of the system remain unclear.

In this Letter we report on a mathematical model capturing entire self-assembly dynamics in a system of magnetic microparticles on the water-air interface. The model is formulated in terms of the Navier-Stokes equation for fluids in a shallow water approximation coupled to interacting magnetic particles described by the corresponding Newton equations. The particles-fluid coupling

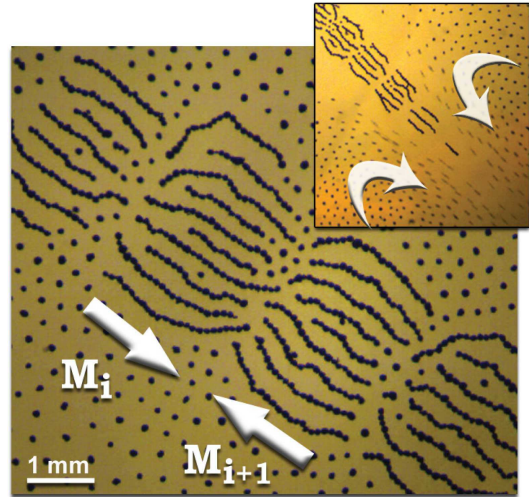


FIG. 1. (Color online): Self-assembled magnetic snake generated by an *ac* field ( $f = 50$  Hz,  $H_0 = 100$  Oe), composed of  $90\mu\text{m}$  Nickel spheres: individual particles form self-assembled ferromagnetic chains which in turn align in segments of the snake. Arrows show the orientation of the total magnetic moments in the segments. *Inset*: Pair of counter-rotating vortices at the tail of a magnetic snake.

is two-fold: an external *ac* magnetic field causes oscillations of the particles and deformations of the air-fluid interface. In turn, hydrodynamic flows advect/reorient particles and thus mediate magnetic dipole interactions. Our numerical studies faithfully reproduce observed phenomenology: formation of dynamic snake-like arrangements of magnetic particles from initially disordered configurations, complex ferromagnetic-antiferromagnetic ordering of the snake, quadrupole structure of self-generated vortex flows, and even self-propulsion of a bead-snake hybrid. The computational algorithm is implemented for graphics processing units (GPUs). Insight and techniques developed in the course of this work can be applied to a variety of non-equilibrium interfacial non-

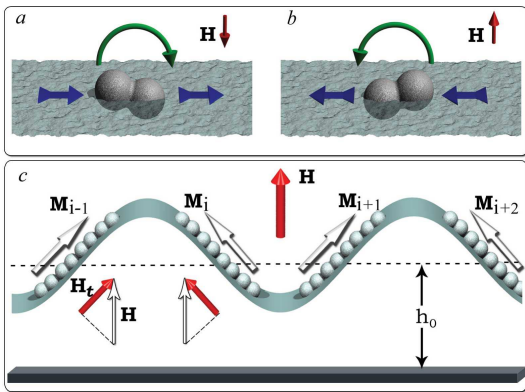


FIG. 2. (Color online): (a), (b): Surface flows generated by dimers/short chains due to external torques exerted by a vertical *ac* magnetic field. (c): coupling between chains and surface deformations. White arrows indicate the magnetic moment orientations in segments.  $H_t$  is a tangential component of the external *ac* field enforcing a specific orientation of the chain's magnetic moment.

equilibrium systems with competing interactions.

A precise description of the motion of particles suspended on the air-water interface is computationally prohibitive. In particular, accurate modeling of the three-dimensional finite Reynolds number (*Re*) Navier-Stokes equation (snakes have  $\text{Re} \approx 100$ ), realistic account for particle-fluid interaction and description of solid-fluid contact lines required enormous computational power. Here we propose a simplified yet nontrivial model allowing for the investigation of the entire process of the snakes' self-assembly. The model identifies key physical mechanisms and ingredients. We made the following major approximations: (i) we considered the Navier-Stokes equation in the so-called shallow water limit (see, e.g. [15]). This approximation is valid when the characteristic length of the snake is large compared to the thickness of the fluid layer  $h_0$ . We verified independently in our experiments that the snakes exist on thin layers of liquid. (ii) We simplified the magnetic interaction between particles by restricting orientation of their magnetic moments along the surface of the fluid. This implies that the "elementary" object in our description is a microchain or a magnetic dimer formed by two spherical ferromagnetic particles (the magnetic moment of the chain is directed along the chain). (iii) We simplified the particle-fluid interaction by assuming that the primary effect of the vertical *ac* magnetic field is a rocking motion of the particles leading to the generation of surface flows, see Fig. 2a,b. We took into account advection of particles by surface flows and rotation of their orientation due to vorticity and shear. However, we neglected hydrodynamic flows due to in-plane drift and rotation of the particles: for the conditions of our experiments, the magnitude of these motions is substantially smaller than those produced by

the external magnetic field.

The evolution of the fluid surface  $h$  and the depth-averaged hydrodynamic velocity  $\mathbf{v}$  is described by

$$\partial_t h + \nabla(h\mathbf{v}) = 0, \quad (1)$$

$$\partial_t \mathbf{v} + (\mathbf{v}\nabla)\mathbf{v} = \eta(\nabla^2 \mathbf{v} - \xi \mathbf{v}) - \nabla h + \sigma \nabla \Delta h + H_0 \sin(\omega t) \sum_j s(\mathbf{r} - \mathbf{r}_j) \mathbf{p}_j \quad (2)$$

where  $\eta$  is the kinematic viscosity;  $\sigma$  the surface tension; the term  $-\xi \mathbf{v}$  describes friction with the bottom of a container (we used  $\xi = 3$  for laminar flow). Eq. (2) is linearized near the equilibrium height  $h_0$ . The variables are scaled as follows: coordinates  $\mathbf{r} \rightarrow \mathbf{r}/h_0$ , time  $t \rightarrow t\sqrt{h_0/g}$ , velocities  $\mathbf{v} \rightarrow \mathbf{v}/\sqrt{gh_0}$ , where  $g$  is the gravitational acceleration. The last term in Eq. (2) describes the forcing on the fluid induced by motion of particles in the applied *ac* magnetic field with the magnitude  $H_0$  and frequency  $\omega$ . Here,  $\mathbf{p} = (\cos(\phi), \sin(\phi))$  is a unit orientation vector parallel to the particle's magnetic moment and  $s(r)$  is a function describing the shape of the particle. In most of our simulations we used:  $s = A_0 \exp(-r^2/s_0^2)$  for  $r < r_0$  and  $s = 0$  for  $r > r_0$ , where  $s_0$  is the parameter related to the particle size,  $r_0$  is a cutoff radius, typically 5-7 particles sizes, and the parameter  $A_0$  (set later to  $A_0 = 1$ ) characterizes the strength of the magnetic forcing. Our simulations show that this particular choice of the function  $s$  provides a good coupling between particles and the continuum hydrodynamic field.

Particle positions and orientations  $\mathbf{r}_j, \mathbf{p}_j$  are governed by the following equations [16]

$$m_p \ddot{\mathbf{r}}_j + \mu_t \dot{\mathbf{r}}_j = \mathbf{F}_j + \mu_t \mathbf{v} - \beta \nabla h \quad (3)$$

$$I_p \ddot{\phi}_j + \mu_r \dot{\phi}_j = T_j + \frac{\mu_r \Omega}{2} + \mu_r \epsilon \mathbf{p}_j \cdot \mathbf{E} \cdot (\mathbf{I} - \mathbf{p}_j \mathbf{p}_j) \times \mathbf{p}_j + \kappa H_0 \sin(\omega t) \nabla h \times \mathbf{p}_j \quad (4)$$

where  $m_p$ ,  $I_p$ ,  $\mu_t$ , and  $\mu_r$  are the particle's mass, moment of inertia, translational and rotational viscous drag coefficients, respectively.  $\mathbf{F}_j$  and  $T_j$  are forces and torques due to magnetic dipole-dipole interaction and steric repulsion between the particles (torques have only one non-zero component).  $\Omega = \partial v_y / \partial x - \partial v_x / \partial y$  is the vorticity and  $E_{kl} = (\partial v_k / \partial x_l + \partial v_l / \partial x_k) / 2$  is the rate of the strain tensor of the hydrodynamic flow, and  $\mathbf{I}$  is the identity matrix. While we kept  $\epsilon$  for the sake of completeness – the accelerations  $m_p \ddot{\mathbf{r}}_j, I_p \ddot{\phi}_j$  in the equations of motion, for typical experimental conditions these terms are irrelevant and can be omitted. Eqs. (3)&(4) have the following meaning: in addition to magnetic forces and torques  $\mathbf{F}_j, T_j$ , the particles are subject to advection by the hydrodynamic flow ( $\sim \mathbf{v}$ ), sliding down the gradient of the surface due to gravity ( $\beta \nabla h$ ) and rotation due to the flow's vorticity ( $\sim \Omega$ ). Moreover, anisotropic objects, such as microchains formed by magnetic particles, will tend to align along the axis of the rate of the strain tensor  $E_{kl}$  with a certain prefactor  $\epsilon$  which in turn depends

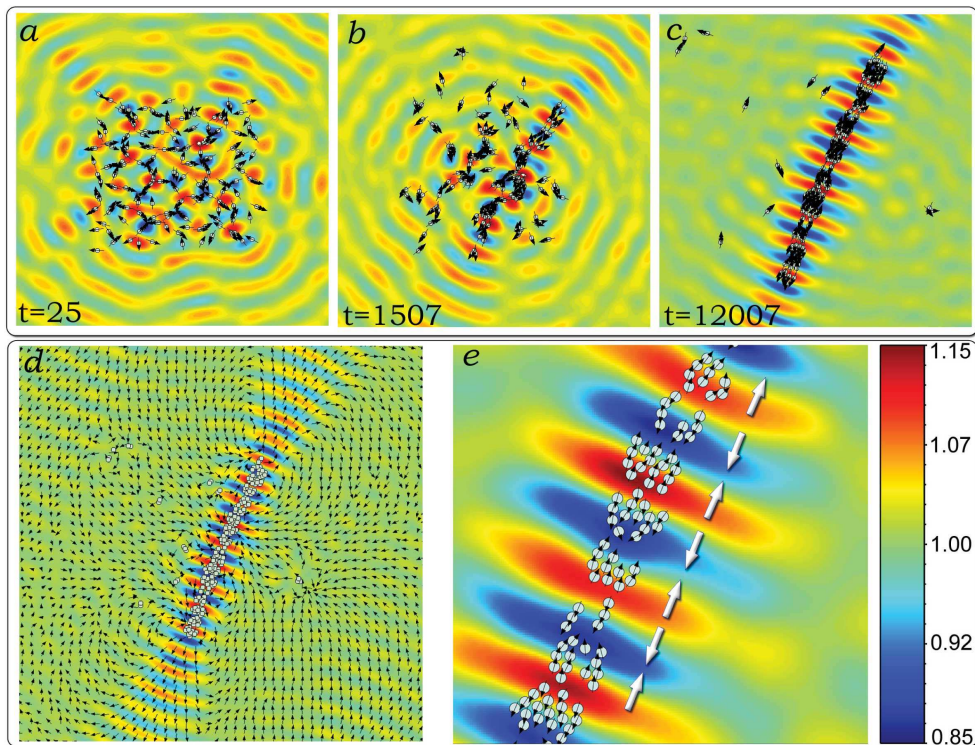


FIG. 3. (Color online): (a)-(c) Formation of a snake from 225 initially randomly distributed particles. The background color represents the height of the fluid surface ( $h$ ), black arrows depict the orientation of the magnetic moments of the particles, and particles are shown as grey circles. Only a part of the entire integration domain is shown. (d) Flows generated by the snake in the entire domain. (e) Antiferromagnetic order between the snake's segments; chains of particles are ferromagnetically ordered in each segment. The parameters of the simulations are: amplitude  $H_0 = 0.56$ , frequency  $\omega = 1$ , layers thickness  $h_0 = 1$ , domain area  $160 \times 160$ , magnetic moment  $\mu_0 = 0.26$ , viscosity  $\eta = 0.01$ , and particle diameter  $a = 0.8$ , and  $\kappa = 3$  (Movies and other parameters are in [17]). These parameters are estimated for the following experimental values: layer depth 1 mm, particles radius 0.4 mm, frequency of the ac field  $f \approx 18$  Hz ( $\omega = 2\pi f$ ), and for the viscosity and surface tension of water.

on the shape of the particle (for spheres  $\epsilon = 0$ ). The last term in Eq. (4) deserves a special attention: it describes the magnetic alignment of particles along the direction of projection of the external  $ac$  magnetic field *parallel* to the surface of the fluid, see Fig. 2c. The in-plane component of the field, oscillating with the same frequency  $\omega$  appears due to the deformation of the surface, and is proportional to  $\nabla h$ . This in-plane field promotes *anti-ferromagnetic* ordering of the neighboring segments and is crucial for the formation of snakes.

The interaction between particles  $j, k$  is described by the Hamiltonian  $\mathcal{H} = \mathcal{H}^d + \mathcal{H}^h$ , where  $\mathcal{H}^d$  is due to the magnetic dipole-dipole interaction,

$$\mathcal{H}^d = -\frac{\mu_0^2}{4\pi r_{jk}^3} [3(\mathbf{p}_j \mathbf{e}_{jk})(\mathbf{p}_k \mathbf{e}_{jk}) - \mathbf{p}_j \mathbf{p}_k], \quad (5)$$

$r_{jk}$  is distance between particles,  $\mathbf{e}_{jk} = \mathbf{r}_{jk}/r_{jk}$ ,  $\mu_0$  magnetic moment of individual particle, and  $\mathcal{H}^h = \mu_0^2 (a/r_{jk})^{24}/16\pi a^3$  models a sufficiently rigid short-range hard-core repulsion between the particles of diameter  $a$  [18]. Correspondingly, forces are evaluated as  $\mathbf{F}_j = -\partial\mathcal{H}/\partial\mathbf{r}_j$  and torques as  $T_j = -\mathbf{p}_j \times \partial\mathcal{H}/\partial\mathbf{p}_j$ .

Equations (1)-(4) were solved in a periodic  $x, y$  domain by a quasispectral method. We used a domain area of  $160^2$  in dimensionless units (the length is normalized by the layer height  $h_0$ ), on a grid with  $1024^2$  points, and up to 225 magnetic particles. The algorithm was implemented for massive parallel GPUs and run on a NVIDIA GTX285 GPU with a peak performance of 1 TFlop. Typically, a speed up more than 100 times was achieved compared to a fast Intel i7 CPU, for details on the implementation of the algorithm see [17].

Figures 3(a)-(c) illustrate the formation of a snake from initially random distributed particles. The result qualitatively reproduces experimental observations: magnetic particles assemble into short chains, then chains form segments consisting of several parallel chains, and finally segments form snakes-like linear objects. Like in experiments, the segments are ordered *anti-ferromagnetically* Fig. 3 (e). We also plotted the mass flux vector  $h\mathbf{v}$  (unlike in an experiment, Eq. (3) does not provide information on the surface velocity). Remarkably, we observed four large vortices at the tails of the snake, see Fig. 3 (d).

We investigated the effect of the amplitude  $H_0$  and

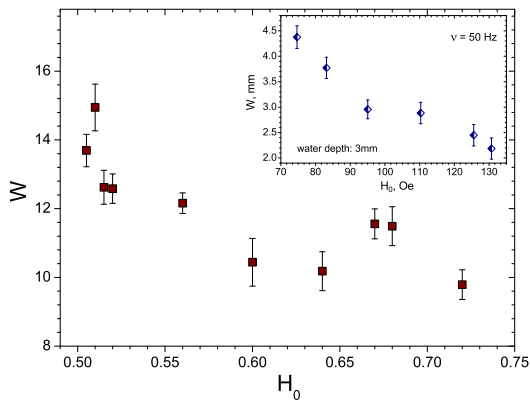


FIG. 4. Snake's width  $W$  vs magnetic field amplitude  $H_0$  in simulations (main plot) and in experiment (inset).

frequency  $\omega$  of the external magnetic field on the snake structure. Good qualitative agreement was obtained: like in experiments (the inset of Fig. 4), we observed a reduction of the snake's width with the increase of  $H_0$ , see Fig. 4. An increase of the amplitude  $H_0$  above a certain threshold resulted in the breakdown of a single snake and formation of multiple snakes with some average length which further decreased with the increase of  $H_0$ , also in agreement with experiments. An increase of the frequency  $\omega$  resulted in a decrease of the segment's size in accordance with the dispersion relation. We also studied the effects of variation of the particle's magnetic moment  $\mu_0$ . We noticed that the snakes are formed only in a certain range of  $\mu_0$ . For small  $\mu_0$  no formation of chains was observed, and for too large  $\mu_0$  the magnetic forces overwhelmed hydrodynamic interactions, and the dominant structures were long chains and closed rings [8].

Our experiment [2] revealed swimmers formed by a snake with a non-magnetic bead. The bead at one of the snake's tails breaks the balance between vortex flows and turns the snake into a self-propelled entity. To verify that, we modified one of the particles in our simulations: the last term  $H_0 \sin(\omega t)$  in Eq. (2) for the last particle was replaced by  $-\eta \zeta_1 v(\mathbf{r}_j)$  (i.e. an increased friction around this particle with a certain friction coefficient  $\zeta_1$ ); also the size of this particle was increased by a factor of 6 compared to magnetic particles. The effect of self-propulsion of a snake with a bead was successfully captured by our model, see Fig. 5. Remarkably, a swimming snake-bead hybrid was formed from random initial conditions: the non-magnetic bead is expelled to the periphery, spontaneously attaches to one of the tails of the snake and forms a swimmer (note asymmetry between the fore and aft vortex pairs).

In conclusion, we developed a microscopic model for self-assembled dynamic magnetic structures at the water-air interface. We identified the minimal ingredients necessary for the description of a highly nontrivial process of dynamic self-assembly. Our work reveals that the snakes

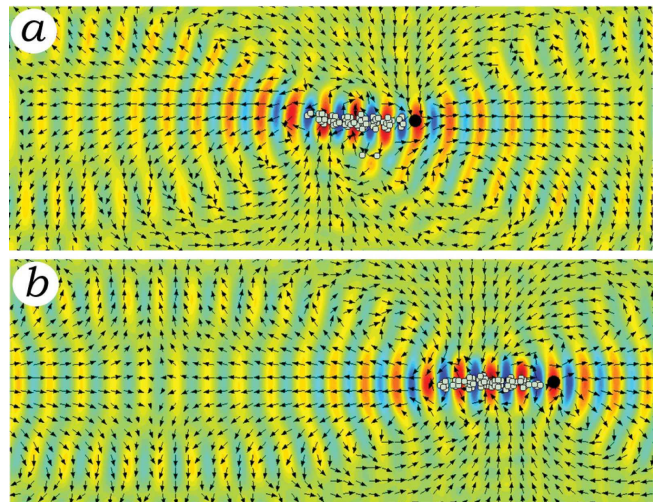


FIG. 5. (Color online): Snake-bead hybrid; the non-magnetic bead is shown as large black circle, the snake consists of 64 particles and  $H_0 = 0.65$  (other parameters as in Fig. 4), see also Movies 2,3 in [17]. The time difference between frames is 85250. (a) and (b) show the same area of the simulated system.

are formed due to a subtle balance between magnetic and hydrodynamic forces. The concepts can be applied to a wide range of interfacial particle systems driven far from equilibrium by external forces, both on the micro and nano scales. The research was supported by the U.S. Department of Energy, Office of Basic Energy Sciences, Division of Materials Science and Engineering, under the Contract No. DE AC02-06CH11357.

- 
- [1] A. Snezhko, I.S. Aranson, W.-K. Kwok, Phys. Rev. Lett.**96**, 078701 (2006); M. Belkin, A. Snezhko, I. S. Aranson, and W.-K. Kwok, Phys. Rev. Lett.**99**, 158301 (2007)
  - [2] A. Snezhko, M. Belkin, I.S. Aranson, W.-K. Kwok, Phys. Rev. Lett.**102**, 118103 (2009)
  - [3] G. Whitesides, B. Grzybowski, Science, **295**, 2418 (2002)
  - [4] S.C. Glotzer, M.J. Solomon, Nature Mat. **6**, 557 (2007)
  - [5] G. Vernizzi and M. Olvera de la Cruz, Proc. Natl. Acad. Sci. USA, **104** 18382 (2007)
  - [6] I.S. Aranson and L.S. Tsimring, Rev. Mod. Phys. **78**,641 (2006); *Granular Patterns*, Oxford Univ. Press, 2009.
  - [7] M. V. Sapozhnikov, Y. V. Tolmachev, I. S. Aranson, and W.-K. Kwok, Phys. Rev. Lett.**90**, 114301 (2003)
  - [8] A. Snezhko, I.S. Aranson, W.-K. Kwok, Phys. Rev. Lett.**94**, 108002 (2005)
  - [9] B. Grzybowski, et al., Appl. Phys. Lett., **84**, 1798 (2004)
  - [10] A. Sokolov, M. M. Apodaca, B. A. Grzybowski, and I. S. Aranson, Proc. Natl. Acad. Sci. USA, **107**, 969 (2010)
  - [11] J. Edd et al., Proceed. of the IEEE/RSJ. Intl. Conf. on Intelligent Robots and Systems, **3**, 2583-2588 (2003)
  - [12] S.T. Chang et al., Nat. Mater, **6**, 235-240 (2007)
  - [13] A. Snezhko, I.S. Aranson, W.-K. Kwok, Phys. Rev. E**73**,

- 041306 (2006)
- [14] M. Belkin, A. Snezhko, I. S. Aranson, and W.-K. Kwok, Phys. Rev. **E80**, 011310 (2009)
- [15] L.D. Landau and E.M Lifshitz, *Fluid Mechanics*, Elsevier, 1987, 552 pp.
- [16] T.J. Pedley, J.O. Kessler, Annu. Rev. Fluid Mech., **24**, 313 (1992)
- [17] See EPAPS Document No. or website <http://mti.msdl.gov/highlights/snakes/index.html>
- [18] A. Hucht, S. Buschmann, P. Entel, Europhys. Lett., **77**, 57003 (2007)